Loading Effect in Copper(II) Oxide Cluster-Surface-Modified Titanium(IV) Oxide on Visible- and UV-Light Activities

ARTICLE *in* THE JOURNAL OF PHYSICAL CHEMISTRY C · NOVEMBER 2013

Impact Factor: 4.77 · DOI: 10.1021/jp4085525

5 AUTHORS, INCLUDING:

Anna Iwaszuk
Tyndall National Institute
14 PUBLICATIONS **166** CITATIONS
SEE PROFILE

Michael Nolan
University College Cork
88 PUBLICATIONS **2,332** CITATIONS
SEE PROFILE

THE JOURNAL OF PHYSICAL CHEMISTRY C

Article

pubs.acs.org/JPCC

Loading Effect in Copper(II) Oxide Cluster-Surface-Modified Titanium(IV) Oxide on Visible- and UV-Light Activities

Qiliang Jin,[†] Musashi Fujishima,[†] Anna Iwaszuk,[‡] Michael Nolan,*[,‡] and Hiroaki Tada*[,†]

[†]Department of Applied Chemistry, School of Science and Engineering, Kinki University, 3-4-1, Kowakae, Higashi-Osaka, Osaka 577-8502, Japan

[‡]Tyndall National Institute, University College Cork, Lee Maltings, Prospect Row, Cork, Ireland

ABSTRACT: $Cu(acac)_2$ is chemisorbed on TiO_2 particles [P-25 (anatase/rutile = 4/1 w/w), Degussa] via coordination by surface Ti−OH groups without elimination of the acac ligand. Post-heating of the $Cu(acac)_2$-adsorbed TiO_2 at 773 K yields molecular scale copper(II) oxide clusters on the surface (CuO/TiO_2). The copper loading amount (Γ/Cu ions nm^{-2}) is controlled in a wide range by the $Cu(acac)_2$ concentration and the chemisorption−calcination cycle number. Valence band (VB) X-ray photoelectron and photoluminescence spectroscopy indicated that the VB maximum of TiO_2 rises up with increasing Γ, while vacant midgap levels are generated. The surface modification gives rise to visible-light activity and concomitant significant increase in UV-light activity for the degradation of 2-naphthol and *p*-cresol. Prolonging irradiation time leads to the decomposition to CO_2, which increases in proportion to irradiation time. The photocatalytic activity strongly depends on the loading, Γ, with an optimum value of Γ for the photocatalytic activity. Electrochemical measurements suggest that the surface CuO clusters promote the reduction of adsorbed O_2. First principles density functional theory simulations clearly show that, at Γ < 1, unoccupied Cu 3d levels are generated in the midgap region, and at Γ > 1, the VB maximum rises and the unoccupied Cu 3d levels move to the conduction band minimum of TiO_2. These results suggest that visible-light excitation of CuO/TiO_2 causes the bulk-to-surface interfacial electron transfer at low coverage and the surface-to-bulk interfacial electron transfer at high coverage. We conclude that the surface CuO clusters enhance the separation of photogenerated charge carriers by the interfacial electron transfer and the subsequent reduction of adsorbed O_2 to achieve the compatibility of high levels of visible and UV-light activities.

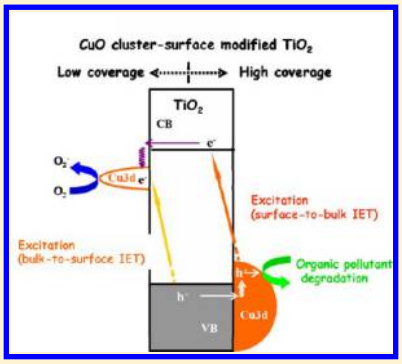

1. INTRODUCTION

Much effort has been devoted to the visible-light activation of TiO_2 for applications as environmental catalysts and self-cleaning materials.[1,2] A conventional approach for the material modification is substitutional cation or anion doping at titanium or oxygen sites.[3−10] Since there are many issues with doping, including solubility, stability, and charge recombination, there is a need to find alternative ways to shift the band gap of TiO_2 in order to make it more efficient in terms of visible-light absorption. Recently, visible-light activation of TiO_2 has been achieved by metal halide and metal ion grafting[11−16] and surface modification with metal oxide clusters.[17−24] Among them, Cu^{2+} ion and CuO have attracted much interest as a promising surface modifier.[25−32] Interestingly, Irie et al. have shown that Cu^{2+}-grafted TiO_2 (Cu^{2+}/TiO_2) prepared by the impregnation method has oxidation ability sufficient for completely decomposing 2-propanol under visible-light irradiation.[28] Even if visible-light activity appears, it is usually much smaller than UV-light activity, and thus, the compatibility of high visible and UV-light activities is important from a viewpoint of effective sunlight use. However, UV-light activity has not been reported for the Cu^{2+}/TiO_2 system and CuO-surface-modified TiO_2. We have recently reported that FeO_x and NiO cluster-surface-modified TiO_2 prepared by the chemisorption−calcination cycle (CCC) technique shows high photocatalytic activities under illumination of visible and UV light.[17−21] In both systems, strong dependence of the photocatalytic activity on the loading amount of the clusters is observed,[17−21] but the reason has not been fully understood.

Herein we show that the surface modification of TiO_2 (P-25, Degussa) with molecular scale copper(II) oxide clusters by the CCC technique (CuO/P-25) causes visible-light activity and a significant increase in the UV-light activity. P-25 (anatase/rutile = 4/1 w/w, specific surface area = 50 $m^2\ g^{-1}$) is known to have the highest level of UV-light activity among commercial TiO_2 and is widely used as a high standard photocatalyst. The strong dependence of the photocatalytic activity on the loading amount of CuO clusters is discussed at an electronic level on the basis of the results from spectroscopic experiments and first principles density functional theory (DFT) simulations.

2. EXPERIMENTAL SECTION

2.1. Catalyst Preparation. TiO_2 particles (anatase/rutile = 4/1 w/w, specific surface area = 50 $m^2\ g^{-1}$, P-25, Degussa) were used as a standard photocatalyst. After TiO_2 particles (2 g) had been added to 200 mL of a $Cu(acac)_2$ acetonitrile solution, they

Received: August 27, 2013
Revised: October 14, 2013
Published: October 16, 2013

   dx.doi.org/10.1021/jp4085525 | J. Phys. Chem. C 2013, 117, 23848−23857

were allowed to stand for 24 h at 298 K. The $Cu(acac)_2$ concentration was changed from 0.1 to 7.0 mM. The solid samples were separated by centrifugation and washed twice with the solvent for the physisorbed complexes to be removed. Then, they were dried in vacuum at room temperature, followed by heating in air at 773 K for 1 h. For electrochemical measurements, mesoporous TiO_2 nanocrystalline film electrodes were used. A paste containing anatase TiO_2 particles with a mean size of 20 nm (PST-18NR, Nikki Syokubai Kasei) was coated on F:SnO_2-film-coated glass substrates (12 Ω/□) by a squeegee method, and the sample was heated in air at 773 K to form mesoporous TiO_2 films (mp-TiO_2/FTO).

2.2. Catalyst Characterization. The Cu loading amount was determined by inductively coupled plasma spectroscopy (ICPS-7510, Shimadzu). The sample (0.1 g) was dispersed to hot concentrated H_2SO_4 (5 mL), and the deposits were thoroughly dissolved into the solution by stirring. The solution was diluted five times in volume with water, and then the Cu concentration was measured. Diffuse reflectance Fourier transform infrared (DRIFT) spectra of the particle samples diluted 25 wt % with KBr (spectroscopic grade, >98%, Kanto Chemical) were obtained with a JASCO FT/IR-470plus spectrometer equipped with a diffuse reflectance attachment (Spectra Tech, Inc.). UV−vis diffuse reflectance spectrum of CuO/TiO_2 was recorded on a Hitachi U-4000 spectrophotometer. Transmission electron microscopic (TEM) observation and energy-dispersive X-ray (ED) spectroscopic measurements were performed using a JEOL JEM-3000F and Gatan imaging filter at an applied voltage of 300 kV. X-ray photoelectron spectroscopic (XPS) measurements were performed using a Kratos Axis Nova X-ray photoelectron spectrometer with a monochromated Al Kα X-ray source ($h\nu$ = 1486.6 eV) operated at 15 kV and 10 mA. The takeoff angle was 90°, and multiplex spectra were obtained for Cu2p photopeaks. All the binding energies (E_B) were referenced with respect to the C1s at 284.6 eV. The electrochemical properties of the CuO/mp-TiO_2/FTO electrodes were measured in 0.1 M $NaClO_4$ aqueous solution in a regular three-electrode electrochemical cell using a galvanostat/potentiostat (HZ-5000, Hokuto Denko). Glassy carbon and a Ag/AgCl electrode (TOA-DKK) were used as a counter electrode and a reference electrode, respectively.

2.3. Photocatalytic Activity Evaluation. Fifty milliliters of 1.0×10^{-5} M 2-naphthol solution (solvent, acetonitrile/water = 1: 99 v/v) or 5.0×10^{-4} M *p*-cresol solution (solvent, water) was placed in a double-jacket-type reaction cell made of borosilicate glass, and then P-25 (Degussa) or CuO/P-25 particles (0.1 g) was added. The reaction cell was irradiated with a Xe lamp (Wacom XRD-501SW) through a band-pass filter (33U, SIGMA KOKI CO., Ltd.) superposed on FTO-coated glass (two pieces of FTO glass for 2-naphthol and a piece of FTO glass for *p*-cresol) transmitting only the 330−400 nm range for the UV photocatalytic activity evaluation and a high-pass filter (L-42, Toshiba) to cut off UV light for the visible-light-induced activity test. The irradiation conditions are as follows: for 2-naphthol UV light ($330 < \lambda < 400$ nm, $I_{320-400\ nm} = 0.5$ mW cm^{-2}) and visible light ($\lambda > 400$ nm, $I_{420-485\ nm} = 1.0$ mW cm^{-2}); for *p*-cresol UV light ($330 < \lambda < 400$ nm, $I_{320-400\ nm} = 2$ mW cm^{-2}) and visible light ($\lambda > 400$ nm, $I_{420-485\ nm} = 2$ mW cm^{-2}). Three milliliters of the solution was sampled every 15 min, and the absorbance at λ = 224 nm was measured using a spectrometer (UV-1800, Shimadzu) to determine the concentration of 2-naphthol. The *p*-cresol concentration was determined by high-performance liquid chromatography [SPD-6A, Shimadzu; column = Fluofix INW425 4.6 × 250 mm (NEOS), mobile phase water−ethanol (3/7 v/v), λ = 277 nm].

2.4. CuO−TiO_2 Calculations. CuO-modified TiO_2 rutile (110) and anatase (001) surfaces are modeled using a three-dimensional periodic slab model with the VASP code.[33] The cutoff for the kinetic energy is 396 eV. The valence electrons are described by a plane wave basis set and include 4 valence electrons for Ti, 6 for O, and 11 for Cu. The exchange-correlation functional is the generalized gradient approximation of Perdew−Wang (PW91).[34,35] We used the Monkhorst−Pack scheme for k-point sampling with a (2 × 2 × 1) sampling grid. The model anatase (001) surface is unreconstructed and is terminated by two-fold-coordinated oxygen atoms while the Ti atoms in the surface layer are five-fold-coordinated. The (110) rutile surface is terminated by two-fold-coordinated bridging oxygen atoms and the next sublayer consists of six-fold- and five-fold-coordinated Ti atoms. We employed a (2 × 4) surface supercell for each TiO_2 surface and a larger (4 × 4) surface supercell for some calculations in order to reduce periodic interactions between adsorbed CuO nanoclusters. The free CuO nanoclusters are calculated in the same supercell as the corresponding CuO-modified TiO_2, and the same technical parameters are used. The clusters were deposited on both TiO_2 surfaces and fully relaxed. The adsorption energy was computed from

$$E_{ads} = E((CuO)_n - TiO_2) - \{E((CuO)_n) + E(TiO_2)\} \quad (1)$$

where $E((CuO)_n - TiO_2)$ is the total energy of the $(CuO)_n$ nanocluster, with n CuO units, supported on the TiO_2 surface. $E((CuO)_n)$ and $E(TiO_2)$ are the total energies of the free $(CuO)_n$ cluster and the bare TiO_2 surface, respectively. A negative adsorption energy signifies that the cluster adsorption is more stable than a separated cluster and surface.

The calculations were carried out using DFT corrected for on-site Coulomb interactions, DFT+U,[36−40] where we applied U = 4.5 eV on the Ti3d states,[41] and for Cu in CuO (with Cu^{2+} states), we apply U = 4 eV, a typical value from the literature.[42] The +U correction results in a relatively good description of the d states in oxidized and reduced Ti and in CuO.

3. RESULTS AND DISCUSSION

The adsorption isotherm of $Cu(acac)_2$ on P-25 from acetonitrile solution was measured at 298 K. As shown in Figure 1A, the adsorption apparently obeys the Langmuir behavior. From the Langmuir plot (inset in Figure 1A), the saturated adsorption amount and the adsorption equilibrium constant were calculated to be 0.54 ions nm^{-2} and 1.34×10^3 M^{-1}, respectively. These results suggest that $Cu(acac)_2$ is chemisorbed on P-25. In the present system, the copper loading amount was expressed by the number of copper ions per unit surface area of TiO_2 (Γ/ions nm^{-2}). Figure 1B shows plots of Γ versus CC cycle number (N) at the initial $Cu(acac)_2$ concentration of 7 mM. The Γ increases with an increase in N. In the CCC technique, the Cu loading amount can be precisely controlled by the $Cu(acac)_2$ concentration at $\Gamma < 0.5$ and by N at $\Gamma > 0.5$.

To further study the mechanism of $Cu(acac)_2$ adsorption on P-25, the absorption spectral change of the solution was traced with adsorption. In the UV range (Figure 2A), $Cu(acac)_2$ and free acetylacetone (Hacac) have absorption bands at 294 and

dx.doi.org/10.1021/jp4085525 | J. Phys. Chem. C 2013, 117, 23848−23857

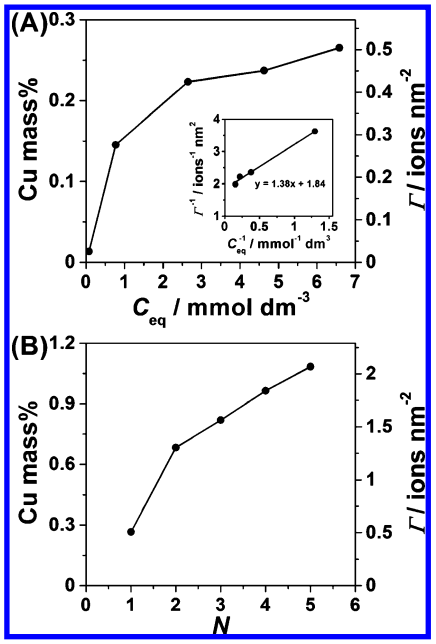

Figure 1. (A) Adsorption isotherm of $Cu(acac)_2$ on P-25 from acetonitrile solution measured at 298 K. The inset shows the Langmuir plot: the *x*-axis denotes the amount of Cu adsorbed per unit mass of TiO_2. (B) Plots of Γ vs chemisorption−calcination cycle number (*N*) ($[Cu(acac)_2]_0$ = 7 mM).

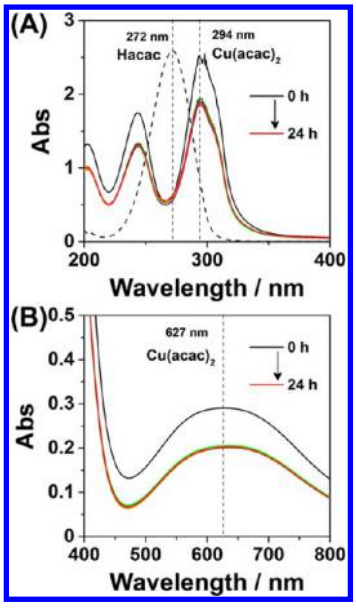

Figure 2. (A) UV (A) and visible (B) absorption spectral change of a $Cu(acac)_2$ solution with adsorption.

272 nm due to the $\pi-\pi^*$ transition, respectively. As the adsorption proceeds, the absorption at 294 nm weakens, but the absorbance at 272 nm is invariant. In the visible range (Figure 2B), there is a weak d−d transition absorption of $Cu(acac)_2$ around 625 nm. The absorption intensity also decreases with adsorption. This finding indicates that $Cu(acac)_2$ is adsorbed on P-25 without liberation of the acac ligand.

To gain information about the states of the adsorbed species before and after heating, diffuse Fourier transform infrared spectra (DRIFT) were measured. Figure 3 shows DRIFT spectra for TiO_2 (a), $Cu(acac)_2/TiO_2$ (b), and $Cu(acac)_2/TiO_2$ heated at 773 K. Spectrum (a) shows that P-25 has an

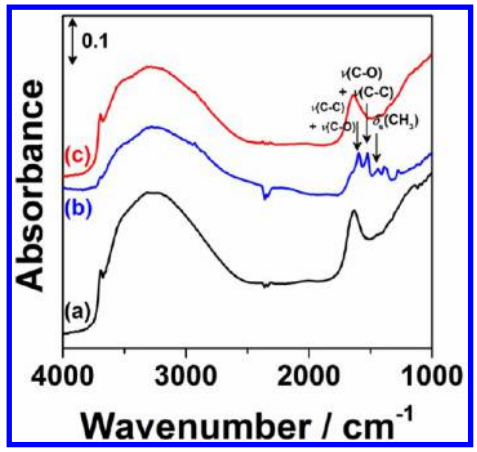

Figure 3. DRIFT spectra for TiO_2 (a), $Cu(acac)_2/TiO_2$ (b), and $Cu(acac)_2/TiO_2$ heated at 773 K (c).

absorption peak due to the surface OH groups (Ti_s-OH) at 3668 cm^{-1},[43] together with a broad absorption of physisorbed water around 3300 cm^{-1}. In spectrum (b), three absorption peaks appear at 1593, 1527, and 1374 cm^{-1}, which can be assigned to the combination of ν(C−C) + ν(C−O), the combination of ν(C−O) + ν(C−C), and $\delta_s(CH_3)$, respectively.[44] Also, the surface OH groups of P-25 (Ti_s-OH) weakens at 3668 cm^{-1}. As shown in spectrum (c), all the absorption peaks of the acac ligands disappear by the heating. These results above suggest that $Cu(acac)_2$ is chemisorbed on P-25 via the chemisorption via surface Ti−OH coordination without elimination of the acac ligands. This is in contrast to the $Fe(acac)_3$ adsorption on TiO_2, which proceeds via the ligand exchange between the acetylacetonate ligand and the surface.[18]

To examine the oxidation state of the copper on the TiO_2 surface, UV−visible absorption spectra of the samples were measured. Cu^{2+}/TiO_2 prepared by the impregnation method has an absorption tail in the 400−500 nm region in addition to the appreciable d−d transition absorption of Cu^{2+} ions at 700−800 nm, whereas the absorption edge is invariant.[28,32] The former weak absorption was assigned to the transition from the VB(TiO_2) to vacant Cu^{2+} ion levels. Figure 4A shows UV−visible absorption spectra of the samples prepared by the CCC technique in the wavelength range from 300 to 800 nm. The d−d transition absorption of Cu^{2+} ions around 750 nm is not observed at $\Gamma \leq 0.28$, whereas the weak absorption appears at $\Gamma \geq 0.32$. Figure 4B magnifies the spectra in the range from 350 to 600 nm to clearly show the shift in the absorption edge with increasing Γ. In contrast to the spectra of Cu^{2+}/TiO_2, band gap narrowing occurs with an absorption tail at 400−500 nm. The absorption spectra are quite different from those of the physical mixtures of P-25 and bulk copper oxides (inset in Figure 4B). The mixture of P-25 with Cu_2O has the interband transition of Cu_2O with a band gap of ∼2 eV[45] and that with CuO has absorption in the whole visible region, without band gap narrowing. These optical features indicate that unique copper oxide species with the oxidation state of +2 are formed by the CCC technique.

Also, X-ray photoelectron spectroscopic (XPS) measurements were performed. Figure 5 shows the Cu2p XP spectra for the copper oxide surface-modified P-25 with varying Γ. In the spectrum for the sample with Γ = 0.015, the signal due to the emission from the $Cu2p_{3/2}$ orbital is observed at the binding

dx.doi.org/10.1021/jp4085525 | J. Phys. Chem. C 2013, 117, 23848−23857

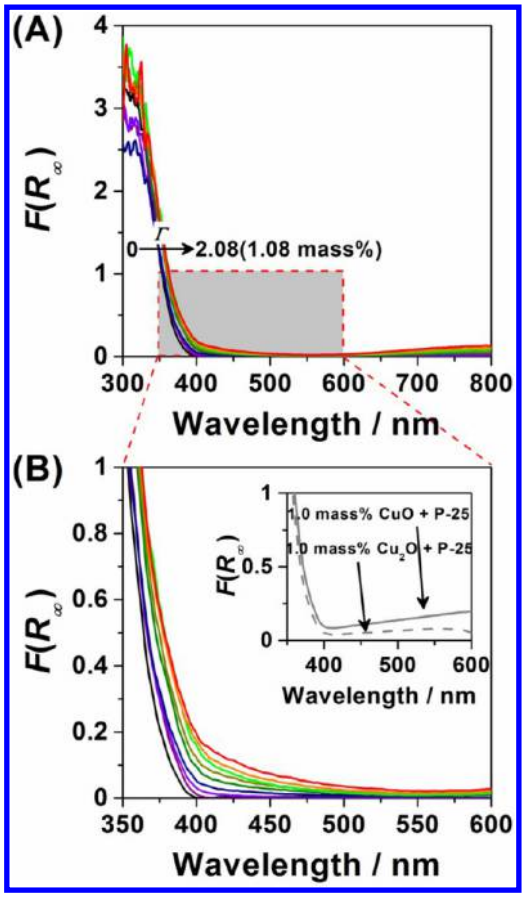

Figure 4. (A) UV−visible absorption spectra of the samples prepared by the CCC technique ($300 < \lambda < 800$ nm): $F(R_\infty)$ denotes the Kubelka−Munk function. (B) Magnified absorption spectra ($350 < \lambda < 600$ nm). For comparison, the spectra of the physical mixtures of P-25 and bulk copper oxides are shown in the inset.

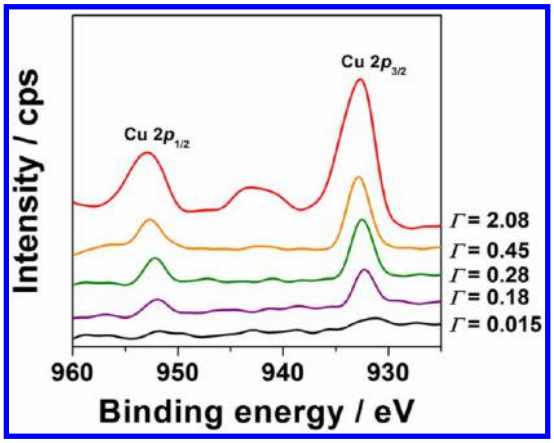

Figure 5. Cu 2*p*-XPS spectra for the CuO-surface-modified P-25 with varying CuO loading (Γ).

energy (E_B) = 931.3 eV. Closer inspection is indicative of a slight shift in the E_B toward higher energy side with increasing Γ. In the spectrum for the sample with Γ = 2.1, the E_B(Cu2p$_{3/2}$) are located at 932.7 eV in addition to a shakeup satellite around 943.1 eV. These E_B values are significantly lower than that for bulk CuO (933.8 eV).[46] It is known that the E_B(Cu2p$_{3/2}$) value shifts to lower binding energy as the loading amount of highly dispersed copper species decreases.[47] The E_B(Cu2p$_{3/2}$) value and the presence of the satellite peak indicate that the copper oxidation state is +2. Evidently, Cu(II) oxide clusters are formed on the TiO_2 surface in a highly dispersion state by the CCC technique. The copper(II) oxide species are formally shown as CuO below.

Figure 6 shows transmission electron micrographs (TEMs) of the samples with Γ < 2.1. No deposits are observed on the P-

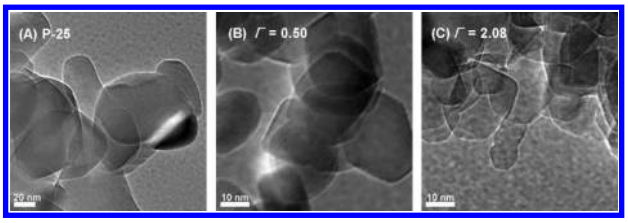

Figure 6. TEMs of the samples with varying Γ prepared by the CCC technique: (A) Γ = 0, (B) Γ = 0.50, (C) Γ = 2.08.

25 surface, whereas CuO particles with a mean size of ∼5 nm are deposited on TiO_2 by the impregnation method.[48] In this manner, extremely small copper oxide clusters are formed on P-25 by the CCC technique. This would result from the strong chemisorption of Cu(acac)$_2$ on P-25 to restrict the growth of the CuO clusters during the postheating process.

2-Naphthol and *p*-cresol are widely used as a starting material of azo dyes and a disinfectant, respectively. For evaluation of the photocatalytic activity of CuO/P-25, 2-naphthol and *p*-cresol with no absorption at $\lambda > 330$ nm were employed as model water pollutants. Both the degradations of 2-naphthol and *p*-cresol apparently followed the first-order rate law under irradiation of UV light ($330 < \lambda < 400$ nm, $I_{320-400\ nm} = 0.5$ mW cm^{-2}) and visible light ($\lambda > 400$ nm, $I_{420-485\ nm} = 1.0$ mW cm^{-2}). The activity was assessed by the pseudo-first-order rate constant (k/h^{-1}). Without photocatalysts or irradiation, the degradations of 2-naphthol and *p*-cresol hardly occurred. Figure 7A shows the rate constants for the 2-naphthol degradation under visible light (k_{vis}/h^{-1}) and UV light (k_{UV}/h^{-1}) as a function of Γ. Significant increases in both the visible- and UV-light activities are induced by the CuO surface modification. The k_{vis} value possesses a maximum of 0.41 h^{-1} at Γ ≈ 0.5. Also, the k_{UV} abruptly increases to 5.8 h^{-1} at Γ ≈ 0.025, which is greater than that for pristine P-25 by a factor of 3.4. While several unidentified intermediates were detected by HPLC, prolonging irradiation time resulted in the complete oxidation of 2-naphthol CO_2. CuO/P-25 appears pale green before the reactions to change red, which suggests that the Cu^{2+} ions in the cluster are partially reduced to Cu^+ ions during the reaction.

On the other hand, Figure 7B shows the k_{vis} and k_{UV} values for the *p*-cresol degradation as a function of Γ. Both the plots exhibit profiles similar to those of the k versus Γ plots for the 2-naphthol degradation, although the enhancing effect by the surface modification is smaller than that for the 2-naphthol degradation.

Valence band (VB) XPS measurements were carried out to examine changes in the filled energy levels of CuO/P-25 with CuO loading. Figure 8A shows the VB-XP spectra for CuO/P-25 with varying Γ. The emission from the VB of TiO_2 primarily consisting of occupied O2p orbitals extends from 2 to 9 eV. As shown in Figure 8B, the VB edge shifts upward by ∼0.7 eV with increasing Γ. The energy of the VB maximum is important because it determines the oxidation ability of the holes—a deep VB edge usually results in good oxidative ability, and increasing

dx.doi.org/10.1021/jp4085525 | J. Phys. Chem. C 2013, 117, 23848−23857

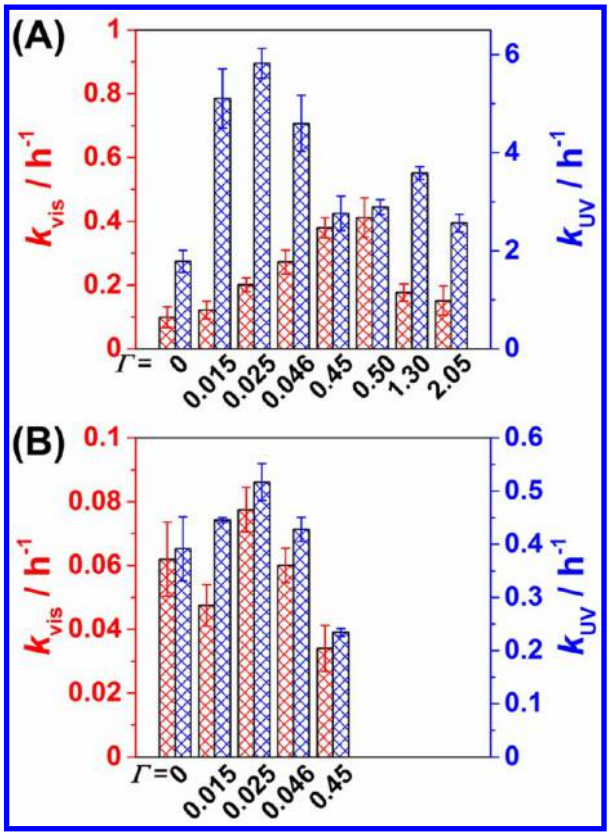

Figure 7. CuO loading (Γ) dependence of the rate constants for the degradations of 2-naphthol (A) and *p*-cresol (B) under irradiation of visible light and UV light.

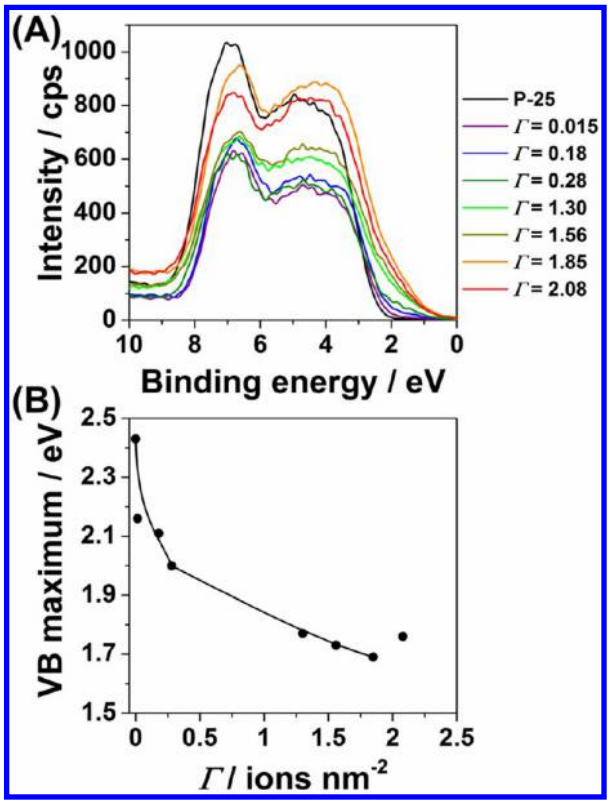

Figure 8. (A) VB-XP spectra for CuO/P-25. (B) Change in the position of the VB maximum level as a function of CuO loading (Γ).

the energy of the VB reduces the oxidative power of the holes. The effective mixing between the surface CuO cluster levels and the O2p states from the surface, as a result of the Ti−O−Cu interfacial bond, is considered to yield a surface d sub-band dispersing around the energy level to overlap with the TiO_2 VB (see DFT simulation). These considerations explain the shift in the VB edge and the band gap narrowing of TiO_2 with CuO modification; that is, the visible-light absorption of CuO/TiO_2 can mainly be attributed to the interfacial electron transfer from the d sunband to the conduction band (CB) of TiO_2. From the band gap for CuO (Γ ≈ 1.9)/P-25 (~1.7 eV), the top of the surface d band is estimated to be situated at +1.8 V versus standard hydrogen electrode (SHE) at pH 7. The electrode potentials are shown with respect to SHE below.

Information about empty levels can be obtained by photoluminescence (PL) spectroscopy. Figure 9 shows PL

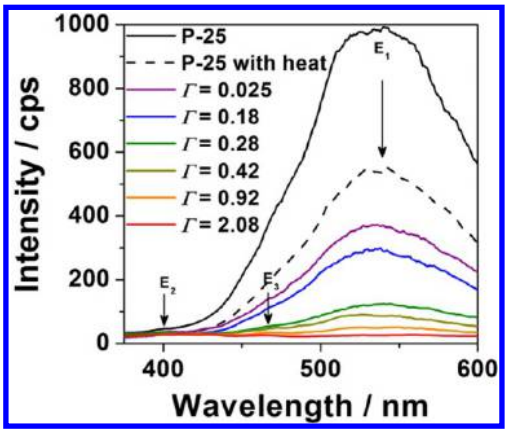

Figure 9. PL spectra of CuO/P-25 with varying CuO loading (Γ) at 77 K: excitation wavelength = 320 nm.

spectra of CuO/P-25 with varying Γ at 77 K. P-25 has a broad emission band around 540 nm (E_1) in addition to the weak band-to-band emission at 400 nm (E_2). The E_1 signal intensity remarkably weakens with heating P-25 at 773 K for 1 h in air. This PL band was assignable to the emission from the surface oxygen vacancy levels of anatase TiO_2,[49] which are healed upon annealing. On modifying P-25 with CuO clusters, the PL intensity gradually decreases with an increase in Γ to disappear at Γ = 2.1. Concomitantly, a weak PL band (E_3) appears near 470 nm, which would arise from the emission from the CuO-derived cluster levels. Consequently, the excited electrons in the CB of TiO_2 are preferentially transferred to the CuO cluster levels rather than the surface oxygen vacancy levels. As suggested by Irie et al., the visible-light-driven transition from the VB of TiO_2 to the vacant CuO cluster levels is also possible (see DFT simulation).[28,32]

Further, the dark current (*I*)−potential (*E*) curves of the mp-TiO_2/FTO and CuO/mp-TiO_2/FTO electrodes were measured in the potential range between −0.4 and +0.4 V in 0.1 M $NaClO_4$ solutions. As shown in Figure 10, for the mp-TiO_2/FTO electrode, only small current flows in the potential range under deaerated conditions. Under aerated conditions, a current peak is observed at −0.3 V, which is close to the potential for one-electron reduction of O_2 ($(E^0(O_2/O_2^-)$ = −0.28 V).[50] On the other hand, for the CuO/mp-TiO_2/FTO electrode, a current peak due to the reduction of the surface Cu(II) oxides to the Cu(I) oxides appears at ~+0.05 V. Interestingly, under aerated conditions, the reduction current

dx.doi.org/10.1021/jp4085525 | J. Phys. Chem. C 2013, 117, 23848−23857

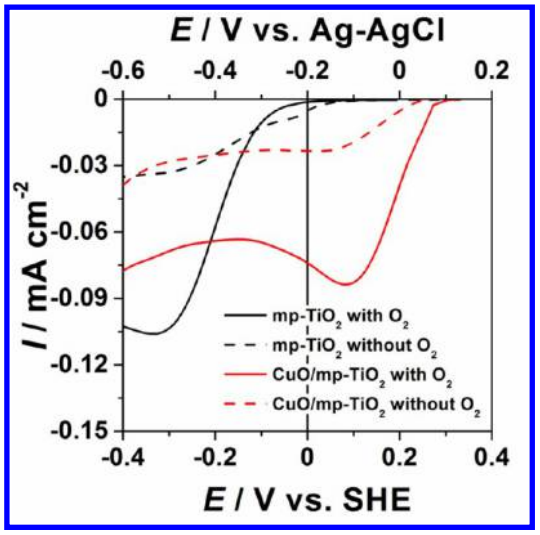

Figure 10. Dark current (I)−potential (E) curves of the mp-TiO_2/FTO and CuO/mp-TiO_2/FTO electrodes measured in 0.1 M $NaClO_4$ solutions.

significantly increases in the potential range from +0.25 to −0.2 V. Nosaka and co-workers have confirmed by means of electron spin resonance spectroscopy and chemiluminescence photometry that visible-light irradiation to Cu^{2+}/TiO_2 yields Cu^+ ions in vacuum and O_2^- ions in water.[32] In the present system, there is a possibility that the interaction between the CuO species and O_2 molecule enhances the O_2 reduction, although multielectron reduction of O_2 cannot be excluded.[28] Thermodynamically, the multielectron reduction is permitted ($E^0(O_2/H_2O_2)$ = +0.68 V and $E^0(O_2/H_2O)$ = +1.23 V), whereas one-electron reduction is impossible. Consequently, the surface Cu(II) oxide species on the TiO_2 surface would be reduced to Cu(I) oxide ones acting as a promoter for the O_2 reduction.

To understand in detail the effect of the surface modification of rutile and anatase by the CuO nanoclusters $(CuO)_n$ at an atomistic level, we have undertaken first principles density functional theory simulations of CuO-nanocluster-modified rutile and anatase surfaces. To study the influence of the Cu loading amount or Γ on the electronic structure of TiO_2, the size of the CuO nanocluster was changed, with CuO, Cu_2O_2, and Cu_4O_4 nanoclusters considered.

Figure 11 shows the atomic structure for rutile TiO_2 modified with $(CuO)_n$ nanoclusters, with n = 1, 2, 4, and the projected electronic density of sates (PEDOS), in which the Cu3d, Ti3d, and O2p EDOS are displayed. Figure 12 shows the atomic structure and PEDOS for anatase (001) modified with $(CuO)_n$ nanoclusters. The Γ values of our models of CuO, Cu_2O_2, and Cu_4O_4 nanoclusters supported on the rutile and anatase surfaces as are follows. On rutile (110): 0.64, 1.28, and 1.78 (on the (4 × 4) surface supercell) Cu atoms/nm^2 and on anatase (001) 0.85, 1.70, and 1.70 (on the (4 × 4) surface supercell) Cu atoms/nm^2.

For both anatase and rutile, the computed adsorption energies in Figures 11 and 12 signify strong adsorption of the CuO nanoclusters at the respective surfaces, driven by formation of new interfacial Cu−O and Ti−O bonds between the cluster and surface and surface and cluster, respectively. For the same cluster size, the energy of adsorption on rutile is larger than that for anatase. This most likely arises from the formation of more interfacial bonds between the CuO nanoclusters and

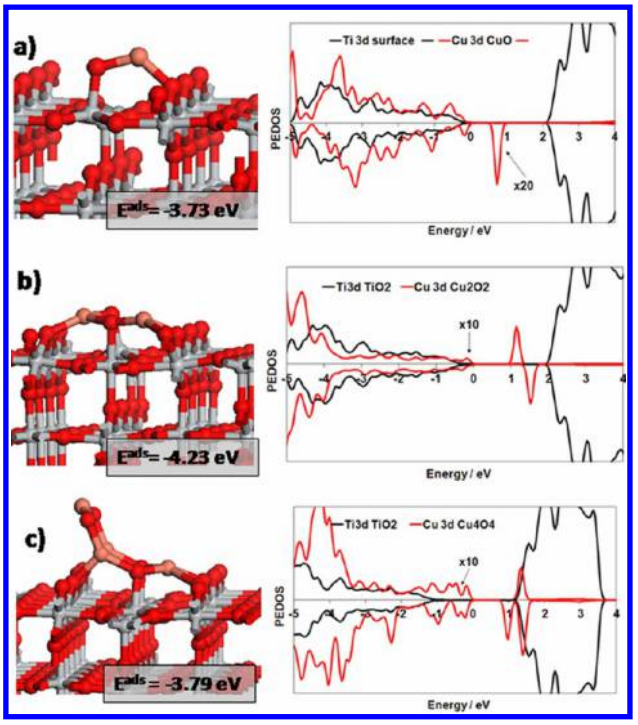

Figure 11. Atomic structure, adsorption energy in eV, and Ti3d and Cu3d projected electronic density of states (PEDOS) for rutile TiO_2 modified with CuO, Cu_2O_2, and Cu_4O_4 clusters.

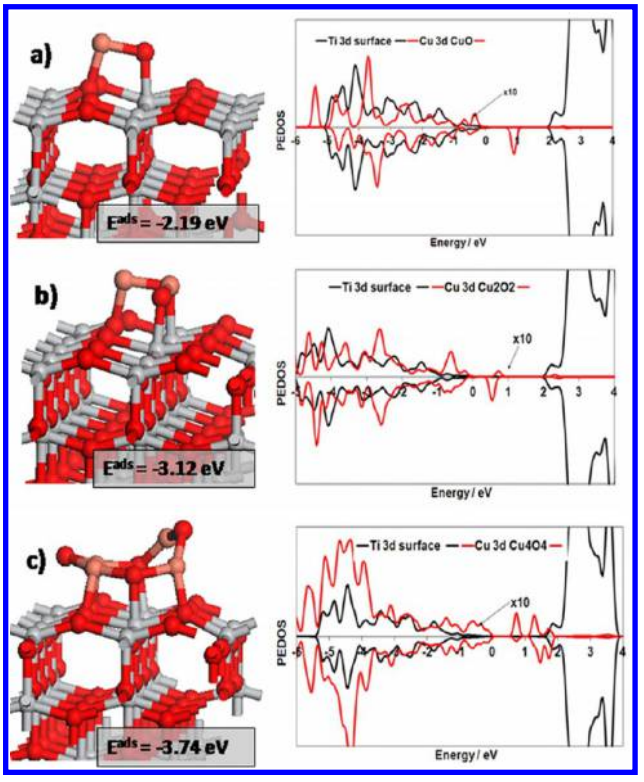

Figure 12. Atomic structure, adsorption energy in eV, and Ti3d and Cu3d projected electronic density of states (PEDOS) for anatase TiO_2 (001) modified with CuO, Cu_2O_2, and Cu_4O_4 clusters.

rutile (110) compared to anatase (001); for example, for $(CuO)_2$, there are four new nanocluster surface bonds at rutile (110) and three at anatase (001). In addition, at anatase (001), one Cu atom in the $(CuO)_2$ nanocluster pulls a two-fold-

dx.doi.org/10.1021/jp4085525 | J. Phys. Chem. C 2013, 117, 23848−23857

coordinated surface oxygen out of the surface, which has an energy cost that reduces the magnitude of the energy gain when the nanocluster interacts with the surface. With the $(CuO)_4$ nanocluster, five new bonds are formed between the nanocluster and both TiO_2 surfaces, with similar adsorption energies.

On rutile (110), the CuO nanocluster has a Cu−O distance to surface bridging oxygen of 1.79 Å, with a Cu−O distance of 1.76 Å in the nanocluster. A surface five-fold-coordinated Ti binds to oxygen from the nanocluster, with a distance of 1.87 Å. The $(CuO)_2$ nanocluster has Cu−O distances to the bridging oxygen in the surface of 1.89 Å for one Cu atom and 1.94 and 2.0 Å for the second Cu. Oxygen atoms from the nanocluster bind to the surface five-fold-coordinated Ti, with Ti−O distances of 1.81 and 2.0 Å. Finally, Cu−O distances in the nanocluster are 1.85, 1.87, and 1.94 Å. We see that the two Cu atoms take different binding environments, with one Cu coordinated to a single bridging oxygen in the surface and two nanocluster oxygens, while the second Cu is coordinated to two bridging oxygen and a single oxygen in the nanocluster. The $(CuO)_4$ nanocluster shows new bonds between three of the nanocluster Cu atoms and the two-fold bridging oxygen of the surface, with Cu−O distances of 1.95, 1.96, and 2.1 Å. The five-fold-coordinated surface Ti atoms bind to two nanocluster oxygen atoms with Ti−O distances of 1.91 Å. Within the nanocluster, the Cu−O distances are in the range of 1.73 Å (for Cu and O not involved in binding to the surface) to 1.93 and 1.95 Å.

On anatase (001), on the CuO nanocluster the Cu atom binds to a two-fold-coordinated surface oxygen atom with a Cu−O distance of 1.91 Å, while oxygen from the nanocluster binds to a surface five-fold-coordinated Ti atom, with a Ti−O distance of 1.80 Å. This oxygen and Ti in the surface are displaced upward, away from the surface layer by 0.17 and 0.34 Å as a result of the interaction with CuO. The Cu−O distance in the nanocluster is 1.76 Å. The $(CuO)_2$ nanocluster shows Cu−O bond to the surface with a distance of 1.80 Å, while oxygen in the nanocluster binds to surface Ti with Ti−O distances of 1.94 and 2.1 Å. Similar to the smaller nanocluster, the surface oxygen and Ti that bind to the nanocluster are displaced out of the surface layer by similar distances. Cu−O distances in the nanocluster are 1.76 and 1.79 Å. Finally, upon adsorption of the $(CuO)_4$ nanocluster, three Cu atoms in the nanocluster form new bonds to the terminal surface oxygen, with Cu−O distances of 1.88, 1.91, and 1.91 Å, with these surface oxygens showing an upward displacement out of the surface layer. Two of the nanocluster oxygen atoms bind to surface Ti sites, with Ti−O distances of 1.94 and 2.03 Å. The Cu−O distances in the nanocluster fall into two groups: in the first, the Cu−O distances are in the range of 1.76−1.78 Å, while in the second group, the Cu−O distances are 1.86−1.89 Å. The first group involves the low-coordinated oxygens that do not bind to the surface, while oxygens that bind to surface Ti fall into the second group.

We examine the PEDOS of surface-modified TiO_2 to gain insights into the effect of CuO nanocluster loading on the energies of the energy bands of TiO_2. It is clear from the PEDOS plots that the surface modification of rutile and anatase by the CuO nanoclusters can cause a significant change in the TiO_2 energy bands at the VB and conduction band (CB) edges, which are strongly dependent on n.

For the modification of rutile (110) with an isolated CuO cluster (n = 1), we find the appearance of unoccupied Cu3d states that are consistent with a Cu^{2+} species in the midgap region. At the same time, the top of VB rises, albeit by a rather small amount. For CuO-modified anatase (001), an unoccupied Cu^{2+} state is also introduced into the midgap region, with some mixing of the CuO VB states with the TiO_2 VB edge. However, in both cases, it is the presence of the unoccupied Cu3d states in Cu^{2+} that is clearly the major effect of the CuO modification. This would be consistent with the interpretation of Irie et al.,[28] in which electrons are excited into these empty CuO states from the occupied TiO_2 VB.

If we now consider the impact of the Cu loading amount on rutile (110), we find interesting behavior in that, as the coverage of CuO increases, there is a significant rise in the top of VB, which is up to ca. 0.7 eV for Cu_4O_4-modified rutile (110). This arises from the presence of CuO-derived occupied states that lie at higher energy than the VB edge of the surface. At the same time, we see that the unoccupied Cu(II)-derived levels undergo an upward energy shift and approach the CB minimum of TiO_2; for example, for Cu_4O_4-modified rutile (110), the unoccupied CuO states lie at the TiO_2 CB edge. While the increase in CuO loading will also result in a narrowing of the band gap compared to unmodified TiO_2, the origin of the band gap narrowing is different; it arises from the upward shift in both the VB and CB edges with increased CuO loading that narrows the band gap. If we now consider the possible fate of excited electrons and holes upon light absorption, then for low CuO loadings, the electron will localize onto the nanocluster, with the hole found on the TiO_2 surface. With increased CuO loading, the electron and hole localization reverses—with electrons localized onto the TiO_2 surface and holes on the CuO nanocluster. This effect suggests that control of CuO loading can be used to tune both the band gap reduction and the nature of the photoexcitation and subsequent activity of photogenerated electrons and holes.

We now consider the PEDOS for anatase (001) modified with CuO nanoclusters, shown in Figure 12. In this case, a similar trend in the nature of the electronic structure is observed in comparison to modified rutile (110), in that the nature of the VB and CB edges depends on the loading amount of CuO clusters, we do find a difference to modified rutile. Comparison of CuO-modified anatase with CuO-modified rutile shows that the unoccupied CuO state is present, but it lies quite deep in the energy gap for rutile and anatase. However, when we consider higher CuO loadings, the empty CuO state persists deep in the energy gap in modified anatase showing a smaller upward shift compared to rutile. At the same time, the upward shift of the VB edge is not as significant as seen for modified rutile. Thus, there is the possibility that both the crystal form of TiO_2 and the loading of CuO can be used to tune the light absorption and subsequent activity of CuO-modified TiO_2.

In the molecular coupling system, the CuO clusters act as an electronic modifier for TiO_2. The action mechanism of the CuO clusters on the photocatalytic activity of P-25 is discussed in detail below. For an isolated CuO cluster (or n = 1), visible-light irradiation can lead to the excitation of the electrons from the VB(TiO_2) to the unoccupied Cu3d levels or the bulk-to-surface interfacial electron transfer as suggested by Irie et al.[28] Although Irie et al. do show a band gap reduction for their CuO clusters grafted by the impregnation method, which are larger than those prepared in the present work, they do not provide any analysis of the origin of the reduced band gap. On the other hand, at $n \geq 2$, the DFT simulations and experimental results

show clearly that excitation from the occupied surface CuO-derived levels to the CB of TiO_2 or the surface-to-bulk electron transfer will likely dominate. Further evidence for this comes from the upward shift in the VB edge with increasing Γ that tracks the decrease in the energy gap with CuO cluster loading. Similar shifts in the VB edge for other metal oxide/nanocluster-modified TiO_2 are explained on the basis of the formation of new VB states coming from the oxide nanocluster.[17−21] This interfacial electron transfer causes efficient charge carrier separation contributing to the increases in the photocatalytic activities and the reduction in the TiO_2-derived PL signal. In the cathodic process, the excited electrons in the CB of TiO_2 can be transferred to the surface CuO cluster levels, which enhances the electron transfer to O_2. Recently, we have shown that the TiO_2-photocatalyzed degradations of 2-naphthol and *p*-cresol proceed via the direct hole oxidation.[51] In the anodic process, the holes in the VB of isolated CuO cluster-surface-modified TiO_2 possess strong oxidation ability to decompose organic compounds including 2-naphthol and *p*-cresol. As the Γ increases, the visible-light absorption intensifies, whereas the rise in the VB maximum weakens the oxidation ability of the holes or the surface nonradiative recombination of the charge carriers may be enhanced. The balance between them would determine the optimum loading amount.

Recently, CuO-nanoparticle-loaded TiO_2 (CuO NP/TiO_2) has attracted much interest because of its photocatalytic activity for hydrogen generation from water containing sacrificial agents such as methanol and glycerol.[52,53] However, to our knowledge, there is no report on the CuO NP/TiO_2-photocatalyzed gradation of organic pollutants. In the nanocoupling system, the band energy of each component is essentially invariant. The flatband potentials of bulk CuO are situated at 0.32 ± 0.01 V at pH 7.[54,55] Thus, the electron transfer from the CB(CuO) to O_2 is impossible if that to H^+ can be rendered possible by the Fermi energy upward shift.[52] Actually, the photocatalytic activity of CuO/TiO_2 significantly decreases even at Γ > 0.5, as shown in Figure 7. Consequently, the contribution of the excitation of the CuO cluster itself to the photocatalytic activity should be minor in the present molecular coupling system.

4. CONCLUSIONS

The CCC technique using $Cu(acac)_2$ as a precursor has formed molecular scale CuO clusters on the surfaces of TiO_2 particles (P-25, Degussa) in a highly dispersed state. Band gap narrowing occurs as a result of the surface modification with a very weak absorption due to the d−d transition. Also, visible-light activities for the degradations of 2-naphthol and *p*-cresol are induced concomitantly with the UV-light activities significantly increased. DFT simulation has indicated that the TiO_2 surface modification by a small amount of isolated CuO clusters yields unoccupied Cu3d levels in the midgap region with the VB maximum hardly changed. However, as the loading amount increases, the experiments and simulations show that the VB maximum rises, and furthermore, the simulations show that the unoccupied Cu3d levels approach the CB minimum, thus giving a different mechanism for band gap reduction. The enhanced visible-light absorption and increased charge separation efficiency lead to a remarkable increase in the photocatalytic efficiency with the CuO nanoclusters acting as a promoter for the reduction of O_2.

AUTHOR INFORMATION

Corresponding Author

*E-mail: h-tada@apch.kindai.ac.jp.

Notes

The authors declare no competing financial interest.

ACKNOWLEDGMENTS

H.T. acknowledges supports from the Ministry of Education, Science, Sport, and Culture, Japan through a Grant-in-Aid for Scientific Research (C) No. 24550239, and Nippon Sheet Glass Foundation for Materials Science and Engineering, and by Sumitomo Foundation. M.N. and A.I. acknowledge support from Science Foundation Ireland (SFI) through the Starting Investigator Research Grant Program, project "EMOIN", Grant No. SFI 09/SIRG/I1620, and the European Commission through the COST Action CM1104 "Reducible Metal Oxides, Structure and Function". We acknowledge access to computing resources at Tyndall provided by SFI and by the SFI and Higher Education Authority funded Irish Centre for High End Computing and the European Commission Partnership in Advanced Computing (PRACE, Contracts RI-261557, RI-283493, and RI-312763) for access to the JUROPA Computer at Forschungszentrum Juelich through the DECI-9 initiative.

REFERENCES

(1) Fujishima, A.; Zhang, X.; Tryk, D. A. TiO_2 Photocatalysis and Related Surface Phenomena. *Surf. Sci. Rep.* **2008**, *63*, 515−582.

(2) Hashimoto, K.; Irie, H.; Fujishima, A. TiO_2 Photocatalysis: A Historical Overview and Future Prospects. *Jpn. J. Appl. Phys.* **2005**, *44*, 8269−8285.

(3) Asahi, R.; Morikawa, T.; Ohwaki, T.; Aoki, K.; Taga, Y. Visible-Light Photocatalysis in Nitrogen-Doped Titanium Oxides. *Science* **2001**, *293*, 269−271.

(4) Khan, S. U. M.; Al-Shahry, M.; Ingler, W. B., Jr. Efficient Photochemical Water Splitting by a Chemically Modified n-TiO_2. *Science* **2002**, *297*, 2243−2245.

(5) Serpone, N. Is the Band Gap of Pristine TiO_2 Narrowed by Anion- and Cation-Doping of Titanium Dioxide in Second-Generation Photocatalysts? *J. Phys. Chem. B* **2006**, *110*, 24287−24293.

(6) Zhang, H.; Chen, G.; Bahnemann, D. W. Photoelectrocatalytic Materials for Environmental Applications. *J. Mater. Chem.* **2009**, *19*, 5089−5121.

(7) Anpo, M.; Takeuchi, M. The Design and Development of Highly Reactive Titanium Oxide Photocatalysts Operating under Visible Light Irradiation. *J. Catal.* **2003**, *216*, 505−516.

(8) Kitano, M.; Funatsu, K.; Matsuoka, M.; Ueshima, M.; Anpo, M. Preparation of Nitrogen-Substituted TiO_2 Thin Film Photocatalysts by the Radio Frequency Magnetron Sputtering Deposition Method and Their Photocatalytic Reactivity under Visible Light Irradiation. *J. Phys. Chem. B* **2006**, *110*, 25266−25272.

(9) Rajeshwar, K.; de Tacconi, N. R. Solution Combustion Synthesis of Oxide Semiconductors for Solar Energy Conversion and Environmental Remediation. *Chem. Soc. Rev.* **2009**, *38*, 1984−1998.

(10) Liu, G.; Wang, L.; Yang, H. G.; Cheng, H.-M.; Lu, G. Q. Titania-Based Photocatalysts: Crystal Growth, Doping and Heterostructuring. *J. Mater. Chem.* **2010**, *20*, 831−843.

(11) Kisch, H. Semiconductor Photocatalysis: Mechanistic and Synthetic Aspects. *Angew. Chem., Int. Ed.* **2013**, *52*, 812−847.

(12) Kisch, H.; Zhang, L.; Lange, C.; Maier, W. F.; Antonius, C.; Meissner, D. Modified, Amorphous Titania: A Hybrid Semiconductor for Detoxification and Current Generation by Visible Light. *Angew. Chem., Int. Ed.* **1998**, *37*, 3034−3036.

(13) Murakami, N.; Chiyoya, T.; Tsubota, T.; Ohno, T. Switching Redox Site of Photocatalytic Reaction on Titanium(IV) Oxide Particles Modified with Transition-Metal Ion Controlled by Irradiation Wavelength. *Appl. Catal., A* **2008**, *348*, 148−152.

(14) Irie, H.; Miura, S.; Kamiya, K.; Hashimoto, K. Efficient Visible Light-Sensitive Photocatalysts: Grafting Cu(II) Ions onto TiO_2 and WO_3 Photocatalysts. *Chem. Phys. Lett.* **2008**, *457*, 202−205.
(15) Yu, H.; Irie, H.; Shimodaira, Y.; Hosogi, Y.; Kuroda, Y.; Miyauchi, M.; Hashimoto, K. An Efficient Visible-Light-Sensitive Fe(III)-Grafted TiO_2 Photocatalyst. *J. Phys. Chem. C* **2010**, *114*, 16481−16487.
(16) Irie, H.; Shibanuma, T.; Kamiya, K.; Miura, S.; Yokoyama, T.; Hashimoto, K. Characterization of Cr(III)-Grafted TiO_2 for Photocatalytic Reaction under Visible Light. *Appl. Catal., B* **2010**, *96*, 142−147.
(17) Tada, H.; Jin, Q.; Nishijima, H.; Yamamoto, H.; Fujishima, M.; Okuoka, S.-i.; Hattori, T.; Sumida, Y.; Kobayashi, H. Titanium(IV) Dioxide Surface-Modified with Iron Oxide as a Visible Light Photocatalyst. *Angew. Chem., Int. Ed.* **2011**, *50*, 3501−3505.
(18) Jin, Q.; Fujishima, M.; Tada, H. Visible-Light-Active Iron Oxide-Modified Anatase Titanium(IV) Dioxide. *J. Phys. Chem. C* **2011**, *115*, 6478−6483.
(19) Nolan, M.; Iwaszuk, A.; Tada, H. Molecular Metal Oxide Cluster-Surface Modified Titanium(IV) Dioxide Photocatalysts. *Aust. J. Chem.* **2012**, *65*, 624−632.
(20) Jin, Q.; Ikeda, T.; Fujishima, M.; Tada, H. Nickel(II) Oxide Surface-Modified Titanium(IV) Dioxide as a Visible-Light-Active Photocatalyst. *Chem. Commun.* **2011**, *47*, 8814−8816.
(21) Iwaszuk, A.; Nolan, M.; Jin, Q.; Fujishima, M.; Tada, H. Origin of the Visible-Light Response of Nickel(II) Oxide Cluster Surface Modified Titanium(IV) Dioxide. *J. Phys. Chem. C* **2013**, *117*, 2709−2718.
(22) Fujishima, M.; Jin, Q.; Yamamoto, H.; Tada, H.; Nolan, M. Tin Oxide-Surface Modified Anatase Titanium(IV) Dioxide with Enhanced UV-Light Photocatalytic Activity. *Phys. Chem. Chem. Phys.* **2012**, *14*, 705−711.
(23) Jin, Q.; Fujishima, M.; Nolan, M.; Iwaszuk, A.; Tada, H. Photocatalytic Activities of Tin(IV) Oxide Surface-Modified Titanium-(IV) Dioxide Show a Strong Sensitivity to the TiO_2 Crystal Form. *J. Phys. Chem. C* **2012**, *116*, 12621−12626.
(24) Jin, Q.; Arimoto, H.; Fujishima, M.; Tada, H. Manganese Oxide-Surface Modified Titanium(IV) Dioxide as Environmental Catalyst. *Catalysts* **2013**, *3*, 444−454.
(25) Ohno, T.; Murakami, N.; Tsubota, T.; Nishimura, H. Development of Metal Cation Compound-Loaded S-Doped TiO_2 Photocatalysts Having a Rutile Phase under Visible Light. *Appl. Catal., A* **2008**, *349*, 70−75.
(26) Ohko, Y.; Noguchi, H.; Nakamura, Y.; Negishi, N.; Takeuchi, K. Highly Selective Photocatalytic Reduction of NO_2 in Air to NO Using Cu^{2+}-Loaded TiO_2 Thin Films. *J. Photochem. Photobiol., A* **2009**, *206*, 27−31.
(27) Wu, Y.; Lu, G.; Li, S. The Role of Cu(I) Species for Photocatalytic Hydrogen Generation over CuO_x/TiO_2. *Catal. Lett.* **2009**, *133*, 97−105.
(28) Irie, H.; Kamiya, K.; Shibanuma, T.; Miura, S.; Tryk, D. A.; Yokoyama, T.; Hashimoto, K. Visible Light-Sensitive Cu(II)-Grafted TiO_2 Photocatalysts: Activities and X-ray Absorption Fine Structure Analyses. *J. Phys. Chem. C* **2009**, *113*, 10761−10766.
(29) Lalitha, K.; Sadanandam, G.; Kumari, V. D.; Subrahmanyam, M.; Sreedhar, B.; Hebalkar, N. Y. Highly Stabilized and Finely Dispersed Cu_2O/TiO_2: A Promising Visible Sensitive Photocatalyst for Continuous Production of Hydrogen from Glycerol:Water Mixtures. *J. Phys. Chem. C* **2010**, *114*, 22181−22189.
(30) Yu, J.; Hai, Y.; Jaroniec, M. Photocatalytic Hydrogen Production over CuO-Modified Titania. *J. Colloid Interface Sci.* **2011**, *357*, 223−228.
(31) Kitano, S.; Hashimoto, K.; Kominami, H. Photocatalytic Degradation of 2-Propanol over Metal-Ion-Loaded Titanium(IV) Oxide under Visible Light Irradiation: Effect of Physical Properties of Nano-Crystalline Titanium(IV) Oxide. *Appl. Catal., B* **2011**, *101*, 206−211.
(32) Nosaka, Y.; Takahashi, S.; Sakamoto, H.; Nosaka, A. Y. Reaction Mechanism of Cu(II)-Grafted Visible-Light Responsive TiO_2 and WO_3 Photocatalysts Studied by Means of ESR Spectroscopy and Chemiluminescence Photometry. *J. Phys. Chem. C* **2012**, *115*, 21283−21290.
(33) Kresse, G.; Hafner, J. Ab Initio Molecular-Dynamics Simulation of the Liquid-Metal-Amorphous-Semiconductor Transition in Germanium. *Phys. Rev. B* **1994**, *49*, 14251−14269.
(34) Blöchl, P. E. Projector Augmented-Wave Method. *Phys. Rev. B* **1994**, *50*, 17953−17979.
(35) Perdew, J. P.; Chevary, J. A.; Vosko, S. H.; Jackson, K. A.; Pederson, M. R.; Singh, D. J.; Fiolhais, C. Atoms, Molecules, Solids, and Surfaces: Applications of the Generalized Gradient Approximation for Exchange and Correlation. *Phys. Rev. B* **1992**, *46*, 6671−6687.
(36) Morgan, B. J.; Watson, G. W. A DFT + *U* Description of Oxygen Vacancies at the TiO_2 Rutile (110) Surface. *Surf. Sci.* **2007**, *601*, 5034−5041.
(37) Anisimov, V. I.; Zaanen, J.; Andersen, O. K. Band Theory and Mott Insulators: Hubbard *U* Instead of Stoner *I*. *Phys. Rev. B* **1991**, *44*, 943−954.
(38) Dudarev, S. L.; Botton, G. A.; Savrasov, S. Y.; Humphreys, C. J.; Sutton, A. P. Electron-Energy-Loss Spectra and the Structural Stability of Nickel Oxide: An LSDA+U Study. *Phys. Rev. B* **1998**, *57*, 1505−1509.
(39) Ganduglia-Pirovano, M. V.; Hofmann, A.; Sauer, J. Oxygen Vacancies in Transition Metal and Rare Earth Oxides. Current State of Understanding and Remaining Challenges. *Surf. Sci. Rep.* **2007**, *62*, 219−270.
(40) Nolan, M.; Grigoleit, S.; Sayle, D. C.; Parker, S. C.; Watson, G. W. Density Functional Theory Studies of the Structure and Electronic Structure of Pure and Defective Low Index Surfaces of Ceria. *Surf. Sci.* **2005**, *576*, 217−229.
(41) Graciani, J.; Plata, J. J.; Sanz, J. F.; Liu, P.; Rodriguez, J. A. A Theoretical Insight into the Catalytic Effect of a Mixed-Metal Oxide at the Nanometer Level: The Case of the Highly Active Metal/CeO_x/TiO_2(110) Catalysts. *J. Chem. Phys.* **2010**, *132*, 104703/1−104703/8.
(42) Wang, L.; Maxisch, T.; Ceder, G. Oxidation Energies of Transition Metal Oxides within the GGA+U Framework. *Phys. Rev. B* **2006**, *73*, 195107/1−195107/6.
(43) Tada, H. Photoinduced Oxidation of Methylsiloxane Monolayers Chemisorbed on TiO_2. *Langmuir* **1996**, *12*, 966−971.
(44) Nakamoto, K. *Infrared and Raman Spectra of Inorganic and Coordination Compounds*, 4th ed.; Wiley-Interscience: New York, 1986.
(45) Liu, L.; Gu, X.; Sun, C.; Li, H.; Deng, Y.; Gao, F.; Dong, L. In Situ Loading of Ultra-Small Cu_2O Particles on TiO_2 Nanosheets to Enhance the Visible-Light Photoactivity. *Nanoscale* **2012**, *4*, 6351−6359.
(46) Li, G.; Dimitrijevic, N. M.; Chen, L.; Rajh, T.; Gray, K. A. Role of Surface/Interfacial Cu^{2+} Sites in the Photocatalytic Activity of Coupled CuO−TiO_2 Nanocomposites. *J. Phys. Chem. C* **2008**, *112*, 19040−19044.
(47) Chary, K. V. R.; Sagar, G. V.; Srikanth, C. S.; Rao, V. V. Characterization and Catalytic Functionalities of Copper Oxide Catalysts Supported on Zirconia. *J. Phys. Chem. B* **2007**, *111*, 543−550.
(48) Qiu, X.; Miyauchi, M.; Sunada, K.; Minoshima, M.; Liu, M.; Lu, Y.; Li, D.; Sihmodaira, Y.; Hosogi, Y.; Kuroda, Y.; Hashimoto, K. Hybrid Cu_xO/TiO_2 Nanocomposites as Risk-Reduction Materials in Indoor Environments. *ACS Nano* **2012**, *6*, 1609−1618.
(49) Shi, J.; Chen, J.; Feng, Z.; Chen, T.; Lian, Y.; Wang, X.; Li, C. Photoluminescence Characteristics of TiO_2 and Their Relationship to the Photoassisted Reaction of Water/Methanol Mixture. *J. Phys. Chem. C* **2007**, *111*, 693−699.
(50) Denki Kagaku Binran *Handbook of Electrochemistry*, 5th ed.; Electrochemical Society of Japan: Maruzen: Tokyo, 2000.
(51) Praveen Kumar, D.; Shankar, M. V.; Mamatha Kumari, M.; Sadanandam, G.; Srinivas, B.; Durgakumari, V. Nano-Size Effects on CuO/TiO_2 Catalysts for Highly Efficient H_2 Production under Solar Light Irradiation. *Chem. Commun.* **2013**, *49*, 9443−9445.
(52) Kum, J. M.; Yoo, S. H.; Ali, G.; Cho, S. O. Photocatalytic Hydrogen Production over CuO and TiO_2 Nanoparticles Mixture. *Int. J. Hydrogen Energy* **2013**, *38*, 13541−13546.

(53) Deleted in press.
(54) Nakaoka, K.; Ueyama, J.; Ogura, K. Photoelectrochemical Behavior of Electrodeposited CuO and Cu_2O Thin Films on Conducting Substrates. *J. Electrochem. Soc.* **2004**, *151*, C661−C665.
(55) Siegfried, M.; Choi, K.-S. Conditions and Mechanism for the Anodic Deposition of Cupric Oxide Films in Slightly Acidic Aqueous Media. *J. Electrochem. Soc.* **2007**, *154*, D674−D677.